Mathematical and Computational Applications

MDPI

Article

Magneto Mixed Convection of Williamson Nanofluid Flow through a Double Stratified Porous Medium in Attendance of Activation Energy

B. M. Tamilzharasan [1], S. Karthikeyan [1], Mohammed K. A. Kaabar [2], Mehmet Yavuz [3,4,*] and Fatma Özköse [5]

[1] Department of Mathematics, Erode Arts and Science College, Erode 638009, Tamil Nadu, India; mathsmaran365@gmail.com (B.M.T.); skarthi.eac@gmail.com (S.K.)
[2] Institute of Mathematical Sciences, Faculty of Science, University of Malaya, Kuala Lumpur 50603, Malaysia; mohammed.kaabar@wsu.edu
[3] Department of Mathematics and Computer Sciences, Faculty of Science, Necmettin Erbakan University, Konya 42090, Turkey
[4] Department of Mathematics, College of Engineering, Mathematics and Physical Sciences, University of Exeter, Cornwall TR11 2LD, UK
[5] Department of Mathematics, Faculty of Science, Erciyes University, Kayseri 38280, Turkey; fpeker@erciyes.edu.tr
* Correspondence: m.yavuz@exeter.ac.uk or mehmetyavuz@erbakan.edu.tr

Abstract: This article aims to develop a mathematical simulation of the steady mixed convective Darcy–Forchheimer flow of Williamson nanofluid over a linear stretchable surface. In addition, the effects of Cattaneo–Christov heat and mass flux, Brownian motion, activation energy, and thermophoresis are also studied. The novel aspect of this study is that it incorporates thermal radiation to investigate the physical effects of thermal and solutal stratification on mixed convection flow and heat transfer. First, the profiles of velocity and energy equations were transformed toward the ordinary differential equation using the appropriate similarity transformation. Then, the system of equations was modified by first-order ODEs in MATLAB and solved using the bvp4c approach. Graphs and tables imply the impact of physical parameters on concentration, temperature, velocity, skin friction coefficient, mass, and heat transfer rate. The outcomes show that the nanofluid temperature and concentration are reduced with the more significant thermal and mass stratification parameters estimation.

Keywords: Williamson nanofluid; thermal stratification; solutal stratification; mixed convection; Darcy–Forchheimer flow; activation energy

Citation: Tamilzharasan, B.M.; Karthikeyan, S.; Kaabar, M.K.A.; Yavuz, M.; Özköse, F. Magneto Mixed Convection of Williamson Nanofluid Flow through a Double Stratified Porous Medium in Attendance of Activation Energy. *Math. Comput. Appl.* **2022**, *27*, 46. https://doi.org/10.3390/mca27030046

Received: 25 April 2022
Accepted: 23 May 2022
Published: 26 May 2022

1. Introduction

Nanotechnology is the technique of analyzing and separating or adding an object's atoms and molecules that need to be made very small. Over the last thirty years, nanotechnology has significantly impacted vast applications in the petroleum industry, food production, medicine, nuclear energy, cooling of the reactor, and the polymer industry. Primarily, in 1995, Choi and Eastman [1] "coined the term nanofluid by incorporating the substance of nanoparticles into base fluids and theoretically demonstrated their efficiency". Based on their findings, they noticed a considerable increase in the thermal conduction of the base liquid. Buongiorno [2] demonstrated the role of Brownian motion and thermophoresis in a nanofluid. The seven slip mechanisms were studied by Buongiorno and Buongiorno's concepts: inertia, thermophoresis, gravity, Magnus effects, fluid drainage, Brownian diffusion, and diffusionphoresis.

Williamson [3] developed "the flow of Pseudo-plastic equation" and analyzed the properties of the pseudo-plastic flow holding three constants. These are the viscous constant, plasticity constant, and the ratio between the viscous constant and the plasticity constant.

Nadeem et al. [4] tested the Williamson fluid model for 2D flows through a stretching sheet. The role of radiation and heat absorption on an incompressible pseudo-plastic Williamson fluid over the unsteady flow of the boundary layer via a porous stretched surface was explored by Hayat et al. [5] and Karthikeyan et al. [6], and they discovered that increasing the Weissenberg number decreases the skin friction coefficient. According to Zeeshan et al. [7], water- and engine oil-based CNTs flowed through a porous medium. On the other hand, the MHD Williamson fluid flow through a nonlinear curved surface in convective homogeneous and heterogeneous reactions was implemented by K. Ahmed et al. [8]. H. Waqas et al. [9] presented a numerical result for the Carreau–Yasuda nanofluid in a porous medium with bioconvective microorganisms. Nasir Shehzad et al. [10] determined that the suction/injection parameter was generated due to a constant and porous medium in the presence of a heat source, and a chemical reaction was observed. The cutting-edge reports in Williamson nanofluid flow with thermal radiation and heat generation are seen in [11–19].

Cattaneo [20] suggested a modified Fourier's law that included a relaxation time element to overcome the paradox of Fourier's law and heat conduction. Christov [21] extended Cattaneo's theory by including Oldroyd derivatives, and it was named the Cattaneo–Christov model theory. Eswaramoorthi et al. [22] expressed the impact of a Williamson fluid flow of two-dimensional Darcy–Forchheimer on a Riga plate. Dual stratification and a double Catteneo–Christov flux were established for the energy equations. The contribution of Jeffery fluid flow to the non-Fourier heat flux model on a nonlinear stretched surface with double stratification was studied by Hayat et al. [23] and Shankar Goud [24]. Ali et al. [25] used the Cattaneo–Christov dual diffusion model to discuss the 3D incompressible unsteady effect of magneto-hydrodynamics on the transient rotating flow of Maxwell viscous nanofluid. The relation between thermal boundary layer and thermal relaxation time was observed in Abu-hamdeh et al. [26]. Rashid et al. [27] examined the thermal radiation effects of Darcy–Forchheimer Maxwell fluid flow along an exponentially stretching surface with activation energy. Shafiq et al. [28] "reported the influence of convective boundary conditions, thermal radiation and chemical reaction on the three-dimensional flow of Darcy Forchheimer nanofluid across a rotating surface with Arrhenius activation energy". "Entropy formation, activation energy, and binary chemical reaction effects on the Darcy Forchheimer flow of Williamson nanofluid through a nonlinear stretchable flat surface were deliberated" by Ghulam Rasool et al. [29] and Hayat et al. [30].

The activation energy is the smallest quantity of energy forced to trigger a chemical reaction in a system. Energy exists in two types: kinetic and potential. A reaction among molecules could be incomplete due to kinetic energy loss or an inadequate collision. At this point, only the minimum amount of energy is required to initiate the chemical reaction. Bestman [31] was the first to investigate the impact of activation energy on natural action in a permeable boundary layer. Dawar et al. [32] addressed nonlinear stretching plates in magnetohydrodynamics pseudo-plastic nanofluid flow with activation energy. The method of homotopy analysis was performed by Alsaadi et al. [33] to examine the Arrhenius energy equation in the nanomaterial of magneto-Williamson flow. The influence of the activation energy, slip, porosity parameter, and entropy approach on the mixed convective flow of Darcy–Forchheimer along a stretched curved surface was noticed by Muhammad et al. [34]. Danook et al. [35] investigated the mixed convective heat transfer in a turbulent flow of nanofluid. Wasim Jamshed et al. [36] worked on the unsteady flow of a non-Newtonian Casson nanofluid with solar radiation using the Keller box method. The significance of MHD mixed convective flows Casson nanofluids over an elongating irregular surface immersed vertically in a Darcy–Brinkman porous medium was exploited by Alghamdi et al. [37]. Currently, investigators are analyzing the Arrhenius activation energy [38–48]. Other related studies have been conducted in [49–55].

For heat and mass transfer concepts, stratification is an essential component. Due to temperature differences, concentration variations, and differing fluid densities, it happens in inflow distribution. Heat and mass transport occur at the same time in the dual stratifica-

tion process. Natural and mixed convection in a dual stratification medium are essential to study because of their applications. Groundwater reservoirs, industrial food, and regulating hydrogen and oxygen levels in the atmosphere are just a few examples of stratification. Sreelakshmi et al. [56] examined the steady flow of Maxwell fluid Darcy–Forchheimer over a stretching surface with thermal and solutal stratification. Darcy–Forchhemer MHD viscoelastic flow of nanofluid through a nonlinear stretching surface with dual stratification effects was deliberated by Hayat et al. [57]. Eswaramoorthi et al. [58] tested the impact of dual stratification and double non-Fourier heat flux model on the mathematical modeling of a Williamson fluid flow on a Darcy–Forchheimer over a Riga plate. Williamson fluid flow over a stretching in a linear surface was examined by Ahmed et al. [59] Some recent thermal and solutal stratification articles were found in [43–48,56–70].

The vast majority of researchers collaborate on the mixed convective Darcy–Forchheimer flow with the non-Fourier heat flux model via the prescribed boundary layer but have not handled a dual stratified porous medium in Williamson nanofluid. Here, the gap was filled by the Williamson nanofluid on the double Cattaneo–Christov theory, radiation, dual stratification, and the impact of activation energy. The numerical findings were produced using the MATLAB bvp4c approach. Finally, in Williamson nanofluid flow, all the physical parameters were represented by a graphical process. This process is widely used in chemical and thermal engineering fields.

2. Development of the Flow Analysis

Assume a Williamson nanofluid's steady flow through a linearly stretching surface in a Darcy–Forchheimer porous material. The Cattaneo–Christov theory, Arrhenius energy, thermal radiation, and magnetic field are studied. The flow process is revealed by thermal and solutal stratification. Throughout this work, the x and y directions represent velocity components of u and v, respectively (see Figure 1). The surface velocity is presumed to be u_w = ax, where a > 0 denotes the stretching surface rate. The flow equation [69] is as follows:

$$\frac{\partial u}{\partial x}+\frac{\partial v}{\partial y}=0 \tag{1}$$

$$\begin{aligned} u\frac{\partial u}{\partial x}+v\frac{\partial v}{\partial y}=\vartheta\frac{\partial^2 u}{\partial y^2}+\vartheta\sqrt{2}\wedge\frac{\partial u}{\partial y}\frac{\partial^2 u}{\partial y^2}+\frac{\vartheta}{k_f}u+\frac{C_B}{x\sqrt{k_f}}u^2-\frac{\sigma B_0^2}{\rho_f}u \\ +\frac{1}{\rho_f}\left\{\begin{array}{c}(1-c_\infty)g\rho_{f\infty}\Lambda_1(T-T_\infty)\\ -g\left(\rho_p-\rho_{f\infty}\right)(C-C_\infty)\end{array}\right\} \end{aligned} \tag{2}$$

$$\begin{aligned} u\frac{\partial T}{\partial x}+v\frac{\partial T}{\partial y}+\Gamma_T\left(u^2\frac{\partial^2 T}{\partial x^2}+v^2\frac{\partial^2 T}{\partial y^2}+\left(u\frac{\partial u}{\partial x}\frac{\partial T}{\partial x}+v\frac{\partial u}{\partial y}\frac{\partial T}{\partial x}\right)+2uv\frac{\partial T^2}{\partial x\partial y}\right) \\ +u\frac{\partial v}{\partial x}\frac{\partial T}{\partial y}+v\frac{\partial v}{\partial y}\frac{\partial T}{\partial y} \\ =\frac{k_f}{(\rho c)_f}\frac{\partial^2 T}{\partial y^2}+\frac{1}{(\rho c)_f}\frac{16\sigma^* T_\infty^3}{3k_p}\frac{\partial^2 T}{\partial y^2}+\frac{Q_1}{\rho_f C_p}(T-T_\infty) \\ +\tau\left(D_m\left(\frac{\partial T}{\partial y}\right)\left(\frac{\partial C}{\partial y}\right)+\frac{D_n}{T_\infty}\left(\frac{\partial T}{\partial y}\right)^2\right) \end{aligned} \tag{3}$$

$$\begin{aligned} u\frac{\partial C}{\partial x}+v\frac{\partial C}{\partial y}+\Gamma_C\left[u^2\frac{\partial^2 C}{\partial x^2}+v^2\frac{\partial^2 C}{\partial y^2}+\left(u\frac{\partial u}{\partial x}\frac{\partial C}{\partial x}+v\frac{\partial u}{\partial y}\frac{\partial C}{\partial x}\right)+2uv\frac{\partial^2 C}{\partial x\partial y}+u\frac{\partial v}{\partial x}\frac{\partial C}{\partial y}\right. \\ \left.+v\frac{\partial v}{\partial y}\frac{\partial C}{\partial y}\right]=D_m\frac{\partial^2 C}{\partial y^2}+\frac{D_n}{T_\infty}\frac{\partial^2 T}{\partial y^2}-k_r^2(C-C_\infty)\left(\frac{T}{T_\infty}\right)^n exp\left(-\frac{E_A}{kT}\right) \end{aligned} \tag{4}$$

The boundary conditions are

$$\begin{aligned} u=U_w(x)=ax, v=-V_w(x), T=T_w(x)=T_0+bx, C=C_w(x)=C_0+c_1x \quad \text{at} \quad y=0, \\ u\to 0,\ \frac{\partial u}{\partial y}\to 0, T\to T_\infty=T_0+b_1x,\ C\to C_\infty=C_0+c_2x \ \text{ at } y\to\infty \end{aligned} \tag{5}$$

Consider

$$\eta = \sqrt{\frac{a}{\vartheta}}y,\ u = ax\,f'(\eta), v = -\sqrt{a\vartheta}\,f(\eta)\ \theta(\eta) = \frac{T - T_\infty}{T_w - T_0},\ \phi(\eta) = \frac{C - C_\infty}{C_w - C_o} \tag{6}$$

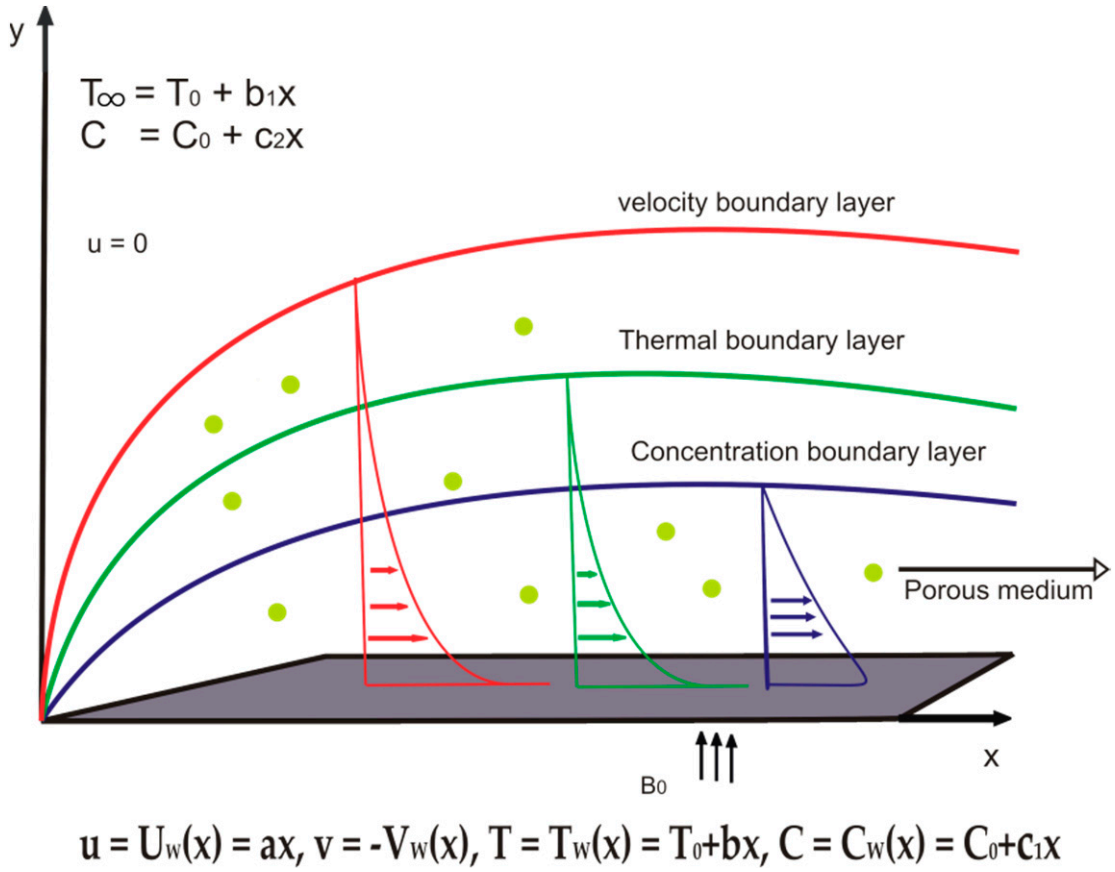

Figure 1. The geometry of the physical model.

Equations (2)–(4) can be modified as follows by using (6):

$$f''' + ff'' - f'^2 + Wif''f''' - Kf' + \lambda(\theta - B_N\phi) - Fcf'^2 - Mf' = 0 \tag{7}$$

$$\begin{aligned}\tfrac{1}{Pr}\left(1 + \tfrac{4}{3}Rd\right)\theta'' - \omega_\theta\left(f^2\theta'' + \theta f'^2 + f'^2S_\theta - ff'\theta' - ff''\theta - ff''S_\theta\right)\\ +N_B\phi'\theta' + N_T\theta'^2 + H_A\theta - f'\theta + f\theta' - S_\theta f' = 0\end{aligned} \tag{8}$$

$$\begin{aligned}\tfrac{1}{SC}\phi'' + f\phi' - \omega_\phi\left(f^2\phi'' - ff''S_\phi - ff''\phi + f'^2\phi + f'^2S_\phi - ff'\phi'\right) - f'\phi + f'S_\phi + \tfrac{N_T}{SCN_B}\theta''\\ -\sigma_o\phi(1 + \theta\delta_o)^n \exp\left(\tfrac{-E}{1+\theta\delta_o}\right) = 0\end{aligned} \tag{9}$$

The boundary conditions are

$$\begin{aligned}\eta \to 0,\ f(0) = fw; f'(0) = 1; \theta(0) = 1 - S_\theta; \phi(0) = 1 - S_\phi\\ \eta \to \infty,\ f'(\infty) = 0; \theta(\infty) = 0; \phi(\infty) = 0\end{aligned} \tag{10}$$

$$E = \tfrac{E_A}{kT_\infty},\ Fc = \tfrac{C_B}{\sqrt{k_f}},\ Gr = \left(\tfrac{(g\beta(1-C_\infty)(T_w-T_\infty)x^3)}{\vartheta^2}\right),\ H_A = \tfrac{Q_1}{\rho_f C_p a},\ fw = -\tfrac{V_w}{\sqrt{a\vartheta}},\ \mathrm{M} = \tfrac{\sigma B_0^2}{\rho_f a},$$
$$Sc = \tfrac{\vartheta}{D_B}, N_B = \tfrac{\tau D_B C_\infty}{\vartheta},\ B_N = \left(\tfrac{(\rho_p - \rho_{f\infty})C_\infty}{\rho_{f\infty}\wedge_1(1-C_\infty)(T_w-T_0))}\right),\ Pr = \tfrac{k_f}{(\rho c)_f},\ Re_x = \tfrac{U_w x}{\vartheta},$$

$Wi = \wedge x\sqrt{\frac{2a^3}{\vartheta}}$, $\lambda = \left(\frac{Gr}{Re_x^2}\right) = \left(\frac{(g\wedge_1(1-C_\infty)(T_w-T_\infty))}{a^2x}\right)$, $N_T = \left(\frac{\tau D_T(T_w-T_0)}{T_\infty\vartheta}\right)$, $R = \frac{4\sigma^*T_\infty^3}{k_pk_f}$, $\delta = \left(\frac{(T_w-T_0)}{T_\infty}\right)$.

Physical quantities for skin friction, Nusselt, and Sherwood number are obtained as follows:

$$C_f = \frac{2\tau_\omega}{\rho U_\omega^2},\ Nu = \frac{xq_\omega}{k_f(\mathrm{T_w}-\mathrm{T_0})},\ Sh_x = \frac{xj_\omega}{D_m(\mathrm{C_w}-\mathrm{C_0})} \tag{11}$$

where

$$\tau_\omega = \mu\left(\frac{\partial u}{\partial y}\left[1+\wedge\sqrt{\tfrac{1}{2}}\frac{\partial u}{\partial y}\right]\right)$$
$$q_\omega = -\left(k_f\frac{\partial T}{\partial y}+\frac{16\sigma^*T_\infty^3}{3k_p}\frac{\partial T}{\partial y}\right)$$
$$j_\omega = -D_m\frac{\partial C}{\partial y}$$

The following are the dimensionless parts of local skin friction, heat, and mass transfer rates.

$$\begin{aligned}\tfrac{1}{2}C_fRe^{\frac{1}{2}} &= f''(0)+\tfrac{Wi}{2}f''(0)^2,\\ Re^{-\frac{1}{2}}Nu &= -\left(1+\tfrac{4}{3}Rd\right)\theta'(0),\\ Re^{-\frac{1}{2}}Sh_x &= -\phi'(0).\end{aligned} \tag{12}$$

3. The Solution Methodology

A system of nonlinear ODEs (7)–(9) with boundary conditions (10) is solved via the MATLAB bvp4c code. The problems are converted into first-order ODEs using the mathematical algorithm described below (Figure 2).

Let $f = y(1)$, $f' = y(2)$, $f'' = y(3)$, $\theta = y(4)$, $\theta' = y(5)$, $\phi = y(6)$, and $\phi' = y(7)$. The following is a list of first-order ODEs:

$$\begin{aligned}
y'(1) &= y(2),\\
y'(2) &= y(3),\\
y'(3) = yy1 &= \left(\tfrac{1}{1+Wi\ y(3)}\right)\\
&\quad *\Big(-y(1)y(3)+y(2)^2+K\,y(2)+Fc\,y(2)^2+M\,y(2)\\
&\quad -\lambda\,(y(4)-B_N\,y(6))\Big),\\
y'(4) &= y(5),\\
y'(5) = yy2 &= \left(\tfrac{1}{1+\left(\frac{4}{3}\right)Rd}-Pr\,\omega_\theta\,y(1)^2\right)\\
&\quad *(-Pr\,y(1)\,y(5)+Pr\,y(2)y(4)+Pr\,S_\theta\,y(2)\\
&\quad +Pr\,\omega_\theta\left(y(4)\,y(2)^2+y(2)^2\,S_\theta-y(1)\,y(2)\,y(5)-y(1)\,y(3)\,y(4)\right.\\
&\quad \left.-y(1)\,y(3)\,S_\theta\right)-Pr\,H_A\,y(4)-Pr\,N_B\,y(7)\,y(5)-Pr\,N_T\,y(5)^2\Big),\\
y'(6) &= y(7),\\
y'(7) = yy3 &= \left(1/\left(1-Sc\,\omega_\phi\,y(1)^2\right)\right)*(-Sc\,y(1)\,y(7)+Sc\,y(2)\,y(6)+Sc\,S_\phi\,y(2)\\
&\quad +Sc\,\omega_\phi\,(y(6)\,y(2)^2+y(2)^2S_\phi-y(1)\,y(2)\,y(7)-y(1)\,y(3)\,y(6)\\
&\quad -y(1)\,y(3)S_\phi)-(N_T/N_B)*yy2\\
&\quad +Sc\,\sigma_o(1+\delta_o\,y(4))^n\,y(6)\,\exp(-E/(1+\delta_o\,y(4))))
\end{aligned}$$

with boundary condition

$$\begin{aligned}
&y0(1) = fw, \quad y0(2) = 1, \quad y0(4) = (1-S_\theta), \quad y0(6) = \left(1-S_\phi\right),\\
&y\mathrm{inf}(2) = 0, \quad y\mathrm{inf}(4) = 0, \quad y\mathrm{inf}(6) = 0
\end{aligned}$$

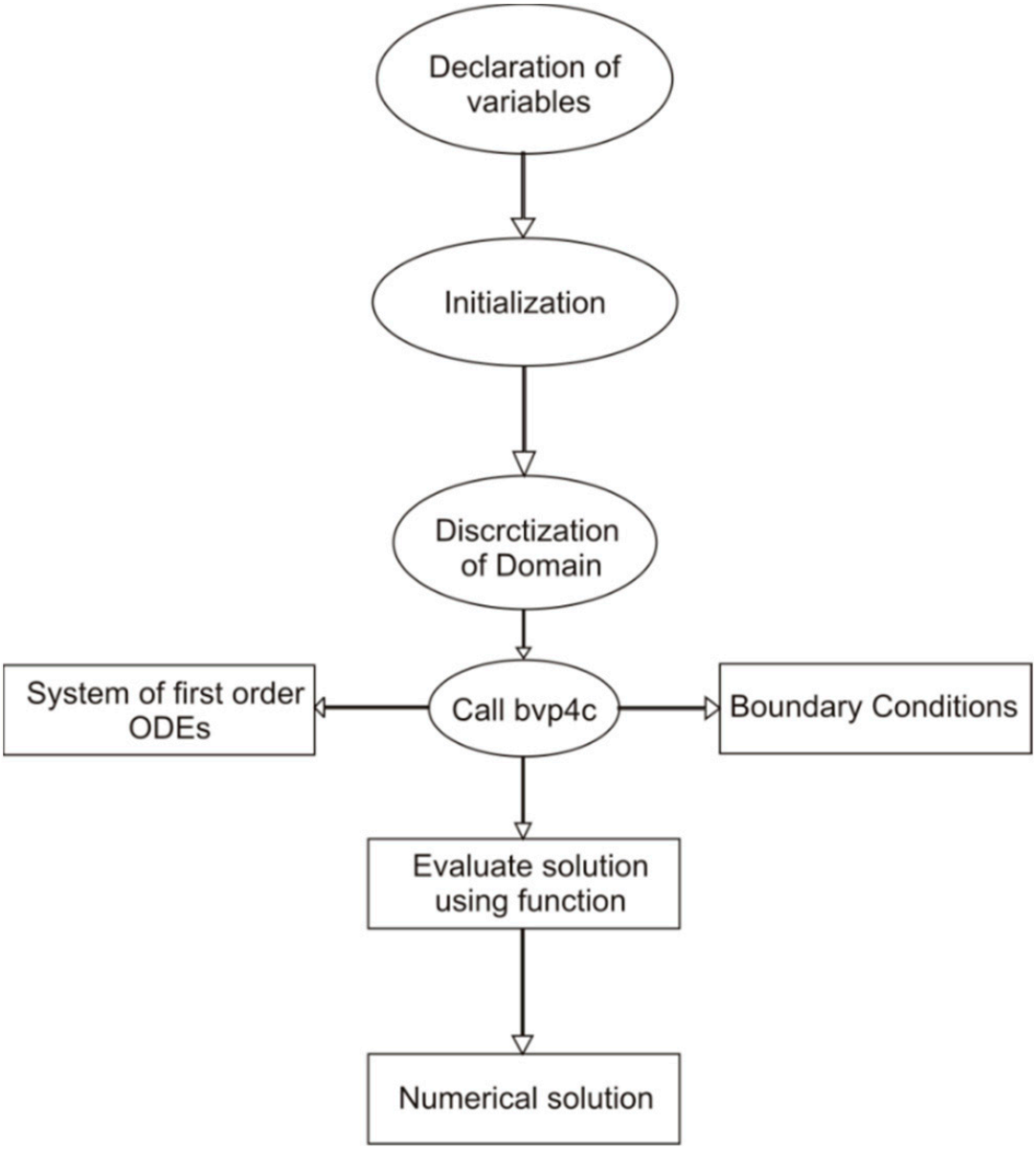

Figure 2. BVP4C computation flowchart.

4. Results and Discussion

Table 1 shows the association between Nusselt numbers taken from Mustafa et al.'s results and our results. We were able to match our results identically to Mustafa's results. The quantitative data of the skin friction drag force ($1/2C_f Re^{1/2}$), heat transfer rate ($NuRe^{-1/2}$), and Sherwood number ($Sh_x Re^{1/2}$) for the several values of Richardson number λ, Weissenberg number Wi, Forchheimer number Fc, Magnetic parameter M, and suction/injection parameter fw were presented in Table 2. Moreover, it was discovered that as Wi and λ values grow, the skin friction coefficient also increases, whereas it was significantly decreased when Fc, fw, and M increased. Tables 3 and 4 incorporated the effects of the embedded parameters Radiation R, Thermal relaxation time parameter ω_θ, Thermal stratification S_θ, Thermophoresis parameter N_T, Mass relaxation parameter ω_ϕ, Mass stratification S_ϕ, and Schmidt number Sc on heat and mass diffusion rates. The higher variation of ω_θ, S_θ, N_T, and S_ϕ was related to the reduced mass and heat transfer rates. It was also accelerated as the thermal radiation, Schmidt number, and mass relaxation time were increased.

Table 1. Correlation of Nusselt number $\left(NuRe^{-\frac{1}{2}}\right)$ when Wi = Fc = K = R = ω_θ = H_A = ω_ϕ = 0, M = B_N = N_B = 0.5, Sc = 5, and δ_0 = 1.

Pr	N_T	E	σ_0	n	λ	$NuRe^{-1/2}$	
						Mustafa et al. [69]	**Present**
2	0.5	1	1	0.5	0.5	0.706605	0.706604
4	0.5	1	1	0.5	0.5	0.935952	0.935955
7	0.5	1	1	0.5	0.5	1.132787	1.132788
10	0.5	1	1	0.5	0.5	1.257476	1.257482
5	**0.1**	1	1	0.5	0.5	1.426267	1.426269
5	**0.5**	1	1	0.5	0.5	1.013939	1.013938
5	**0.7**	1	1	0.5	0.5	0.846943	0.846928
5	**1.0**	1	1	0.5	0.5	0.649940	0.649939
5	0.5	**0**	1	0.5	0.5	0.941201	0.941209
5	0.5	**1**	1	0.5	0.5	1.013939	1.013943
5	0.5	**2**	1	0.5	0.5	1.064551	1.064563
5	0.5	**4**	1	0.5	0.5	1.114549	1.114191
5	0.5	1	**0**	0.5	0.5	1.145304	1.145301
5	0.5	1	**1**	0.5	0.5	1.013939	1.013938
5	0.5	1	**2**	0.5	0.5	0.926282	0.926281
5	0.5	1	**5**	0.5	0.5	0.798671	0.798669
5	0.5	1	2	**−1**	0.5	1.030805	1.030804
5	0.5	1	2	**−0.5**	0.5	0.999470	0.999468
5	0.5	1	2	**0**	0.5	0.964286	0.964285
10	0.5	1	2	**1**	0.5	0.886830	0.886830
10	0.5	1	2	0.5	**0**	1.032281	1.032280
10	0.5	1	2	0.5	**0.5**	1.056704	1.056706
10	0.5	1	2	0.5	**3**	1.154539	1.154538
10	0.5	1	2	0.5	**5**	1.215937	1.215938

Table 2. Numerical analysis of $1/2C_fRe^{1/2}$, $NuRe^{-1/2}$, and $Sh_xRe^{1/2}$ for different parameters Wi, Fc, λ, M, and fw.

Wi	Fc	λ	M	fw	$1/2C_fRe^{1/2}$	$NuRe^{-1/2}$	$Sh_xRe^{-1/2}$
0	0.4	0.5	0.5	0.3	−1.493123	1.667677	0.688683
0.1	0.4	0.5	0.5	0.3	−1.455877	1.661396	0.681731
0.2	0.4	0.5	0.5	0.3	−1.41351	1.653626	0.673835
0.3	0.4	0.5	0.5	0.3	−1.362763	1.643289	0.664469
0.2	0	0.5	0.5	0.3	−1.329383	1.662128	0.682787
0.2	0.2	0.5	0.5	0.3	−1.372209	1.657807	0.678189
0.2	0.4	0.5	0.5	0.3	−1.41351	1.653626	0.673835
0.2	0.6	0.5	0.5	0.3	−1.45342	1.649575	0.669706
0.2	0.4	0	0.5	0.3	−1.470747	1.646644	0.666783
0.2	0.4	0.2	0.5	0.3	−1.44786	1.64946	0.669584
0.2	0.4	0.4	0.5	0.3	−1.424968	1.652245	0.672411

Table 2. *Cont.*

Wi	Fc	λ	M	fw	$1/2C_fRe^{1/2}$	$NuRe^{-1/2}$	$Sh_xRe^{-1/2}$
0.2	0.4	0.6	0.5	0.3	−1.402068	1.655	0.675269
0.2	0.4	0.5	0	0.3	−1.167756	1.642785	0.789742
0.2	0.4	0.5	0.5	0.3	−1.41351	1.653626	0.673835
0.2	0.4	0.5	1	0.3	−1.56368	1.632112	0.646948
0.2	0.4	0.5	1.5	0.3	−1.696232	1.612796	0.626083
0.2	0.4	0.5	0.5	−0.3	−1.13794	1.366538	0.605637
0.2	0.4	0.5	0.5	−0.1	−1.22469	1.476979	0.612521
0.2	0.4	0.5	0.5	0.1	−1.316926	1.576889	0.632016
0.2	0.4	0.5	0.5	0.3	−1.41351	1.653626	0.673835

Table 3. Numerical study of $NuRe^{-1/2}$ for various parameters R, ω_θ, and S_θ.

R	ω_θ	S_θ	$NuRe^{-1/2}$
0	0.1	0.2	1.292138
0.5	0.1	0.2	1.653626
1	0.1	0.2	1.877266
1.5	0.1	0.2	1.926091
0.5	−0.1	0.2	1.64429
0.5	0	0.2	1.662016
0.5	0.1	0.2	1.653626
0.5	0.2	0.2	1.561214
0.5	0.1	0	1.849146
0.5	0.1	0.1	1.753203
0.5	0.1	0.2	1.653626
0.5	0.1	0.3	1.550338

Table 4. Numerical results of $Sh_xRe^{1/2}$ for different parameters Sc, N_T, ω_ϕ, and S_ϕ.

Sc	N_T	ω_ϕ	S_ϕ	$Sh_xRe^{-1/2}$
0.5	0.5	0.1	0.2	0.015548
1	0.5	0.1	0.2	0.673835
1.5	0.5	0.1	0.2	1.186802
2	0.5	0.1	0.2	1.628294
1	0.2	0.1	0.2	1.038076
1	0.3	0.1	0.2	0.911577
1	0.4	0.1	0.2	0.790267
1	0.5	0.1	0.2	0.673835
1	0.5	0	0.2	0.591323
1	0.5	0.1	0.2	0.673835
1	0.5	0.2	0.2	0.759523
1	0.5	0.3	0.2	0.848478
1	0.5	0.1	0	0.899109

Table 4. *Cont.*

Sc	N_T	ω_ϕ	S_ϕ	$Sh_x Re^{-1/2}$
1	0.5	0.1	0.1	0.786382
1	0.5	0.1	0.2	0.673835
1	0.5	0.1	0.3	0.561474

The embedded parameters with fixed values $Wi = 0.2, \delta_o = \omega_\theta = 0.1, \omega_\phi = 0.1$, $\Pr = 2$, $Fc = 0.4, \mathrm{K} = 0.2, \sigma_o = 1, B_N = 0.5, \mathrm{R} = 0.5, H_A = -0.5, N_B = 0.5$, $N_T = 0.5$, $\mathrm{n} = 0.5, fw = 0.3, S_\theta = 0.2, \mathrm{Sc} = 1.0, M = 0.5$, $\lambda = 0.5, E = 1$ and $S_\phi = 0.2$ are existence in velocity f', temperature θ and concentration ϕ profiles. Specifications of the suction/injection parameter fw on velocity field f with the range of $0 \leq \eta \leq 4$ the fluid velocity profile of the nanofluid while comparing the values of Fc and K were noted in Figure 3. In the graph flow between Fc and K, then values of fw varied from $fw = -0.3$ to +0.3 increase, and the velocity profile f' of the graph automatically decreases. The influence of mixed convection parameters λ on the velocity field for various values of the parameters is shown in Figure 4. As shown in Figure 4, the velocity field decays with raising values of $\lambda = 0$ to 0.6. Supporting flow is represented on a warm surface by λ values greater than zero, whereas resisting flow is shown on a cold surface by λ values less than zero. The influence of the Forchheimer number Fc on the velocity profile is seen in Figure 5 for varied $Wi = 0.0$ and 0.4 values. It is determined that the velocity field diminishes when the Forchheimer number rises. The effect of the Weissenberg number Wi on velocity flow is seen in Figure 6 for both magnetic field parameter scenarios. Figure 6 shows that increasing Wi depreciates the velocity field. The relaxation time is prolonged, which restricts fluid motion. The Weissenberg number is used in physical studies of viscoelastic flows to test the impact of elastic to viscous forces. As a result of lowering the velocity of the boundary layer, the Forchheimer number Fc and the porous medium K have different parameter values. In Figures 7 and 8, we present the variation of the Weissenberg number Wi and the magnetic field M of the base flow of the velocity profile. Figures 7 and 8 show that increasing Wi and M lowers the velocity distribution. The Lorentz force is formed when the magnetic field is strengthened. This force aids in reducing the velocity distribution as well as Wi.

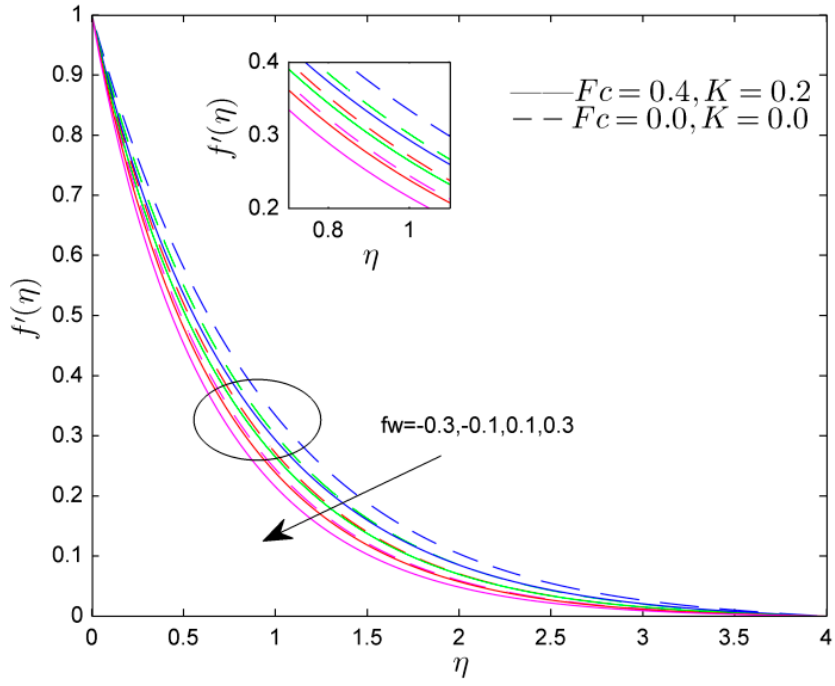

Figure 3. Effect of Suction/Injection parameter (fw) on $f'(\eta)$.

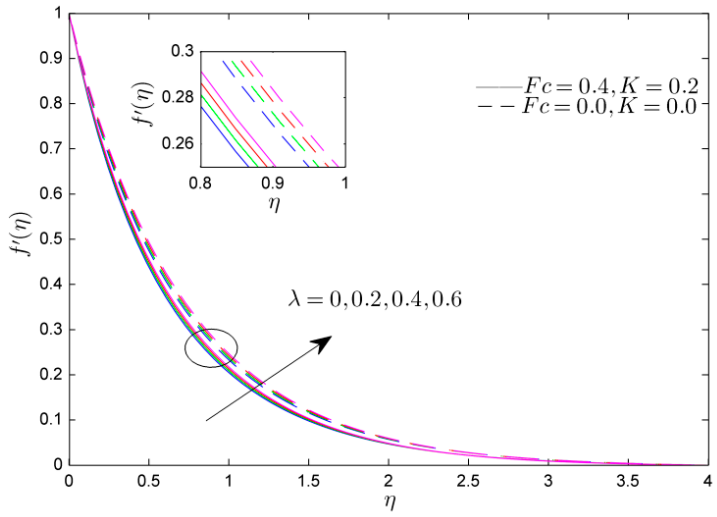

Figure 4. Effect of Richardson number (λ) on $f'(\eta)$.

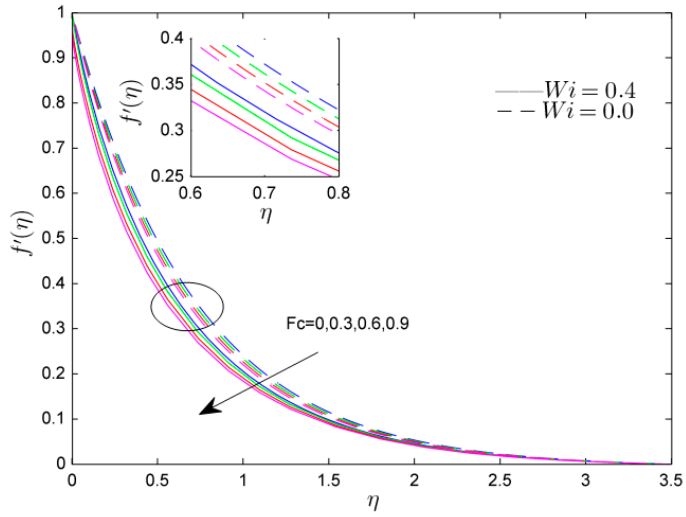

Figure 5. Effect of Forchheimer number (Fc) on $f'(\eta)$.

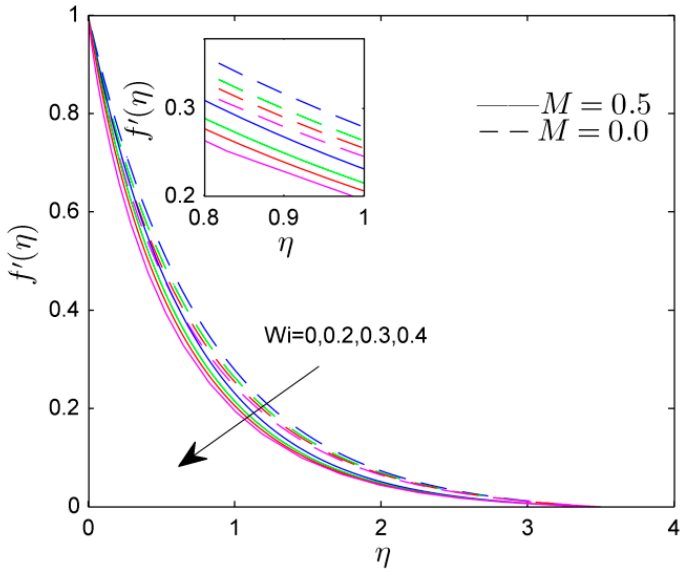

Figure 6. Effect of Weissenberg number (Wi) on $f'(\eta)$ when $M = 0,\ 0.5$.

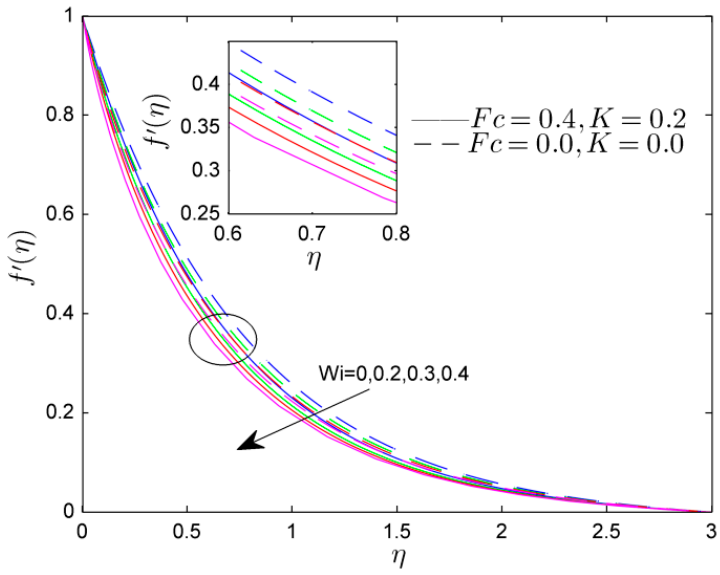

Figure 7. Effect of Weissenberg number (Wi) on $f'(\eta)$ when $Fc = 0,\ 0.4$ and $K = 0,\ 0.4$.

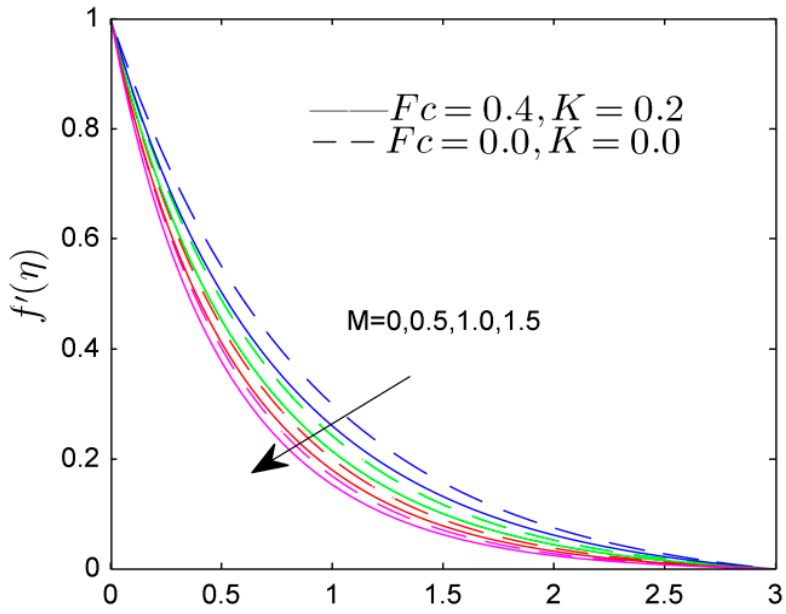

Figure 8. Effect of a Magnetic parameter (M) on $f'(\eta)$.

Specifications of the heat absorption H_A on temperature profile θ within the range of $0 \leq \eta \leq 8$ were established in Figure 9. In the graph, the flow depends on thermal radiation values. When the values of H_A increase, the temperature field also increases. Figure 10 demonstrates the impact of the suction/injection parameter on temperature for different parameters of the Forchheimer number Fc. The temperature field reduces for higher values of fw. Figure 11 reveals the influence of the radiation parameter R on the temperature profile. In these cases, the temperature profile was increased for various values of the thermal radiation grown by varying the thermal relaxation time parameters ω_θ. For various Brownian motion and chemical reaction parameters, Figures 12 and 13 indicate the performance of growing levels of thermal and solutal stratification parameters. The stratification parameter is the ratio of free stream temperature to fluid surface temperature. A significantly larger stratification parameter causes a rise in free stream temperature or a decrease in a nanofluid stream, whereas the concentration profile exhibits the inverse correlation. Temperature and concentration distribution within the boundary layer and

the ambient fluid were reduced as the S_θ and S_ϕ values increased. The profiles of non-dimensional temperature and concentration against thermal relaxation time ω_θ and mass relaxation time parameter ω_ϕ were plotted in Figures 14 and 15. The temperature field shrinks for N_T = 0.0 and 0.5 as ω_θ increases. For $E = 0.0,\ 0.5,$ an upsurge in ω_ϕ decreases the concentration gradient. Figure 16 shows the effect of Sc on the concentration profile with the range of $0 \leq \eta \leq 8$ when $N_T = 0.0$. It was discovered that concentration decreased as Sc increased. Because of this, the Schmidt number has an opposite relation with mass diffusivity. The characteristics of the thermophoresis parameter N_T on the profile of concentration were observed in Figure 17 for S_ϕ = 0.0 and 0.2. The concentration here rises as a function of S_ϕ. The presence of a high value of N_T helps reduce the concentration boundary layer.

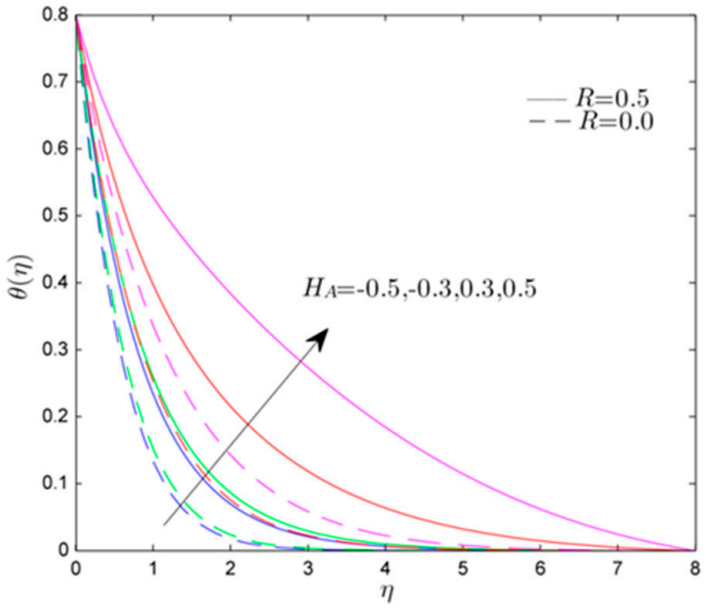

Figure 9. Effect of heat generation parameter (H_A) on $\theta(\eta)$.

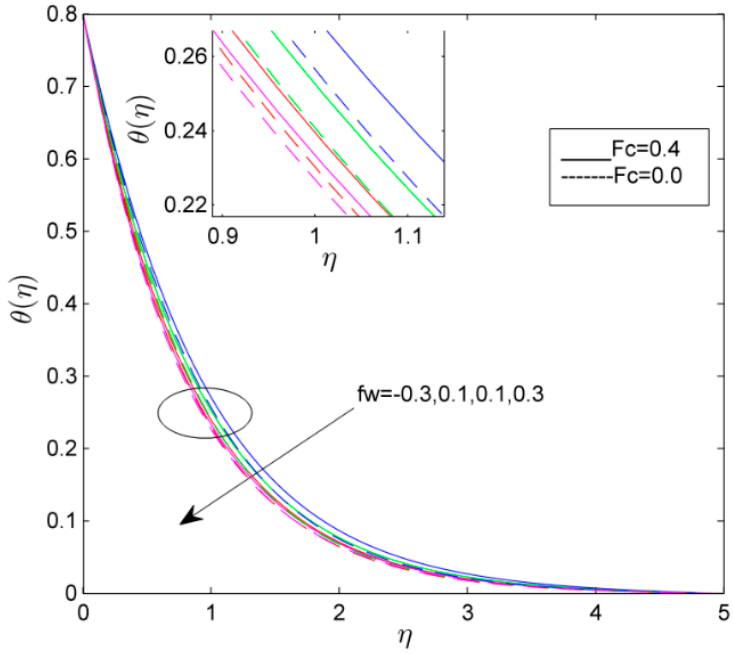

Figure 10. Effect of suction/injection parameter (fw) on $\theta(\eta)$.

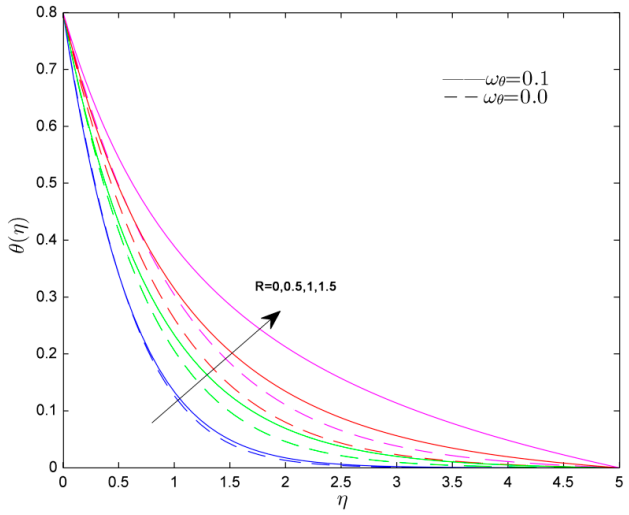

Figure 11. Effect of thermal radiation parameter (R) on $\theta(\eta)$.

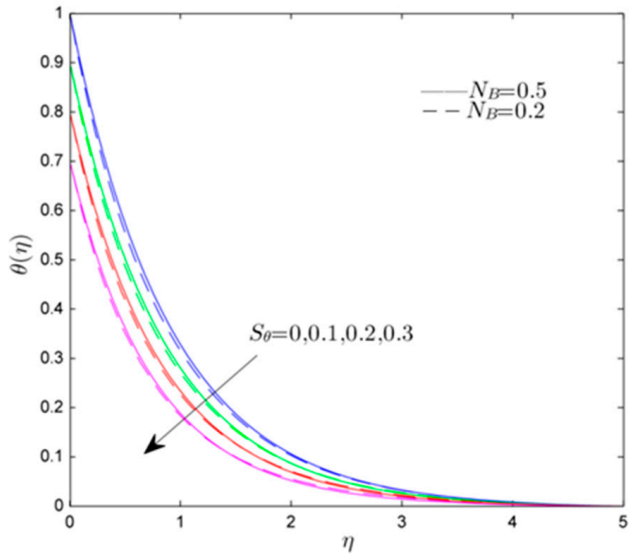

Figure 12. Effect of thermal stratification parameter (S_θ) on $\theta(\eta)$.

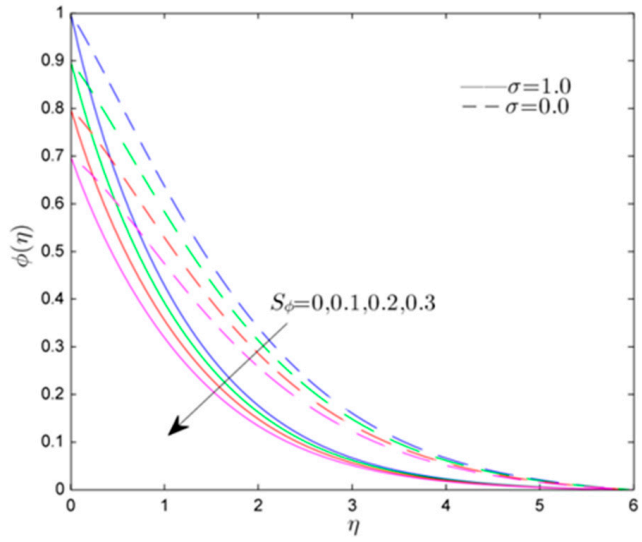

Figure 13. Effect of Solutal stratification (S_ϕ) on $\phi(\eta)$.

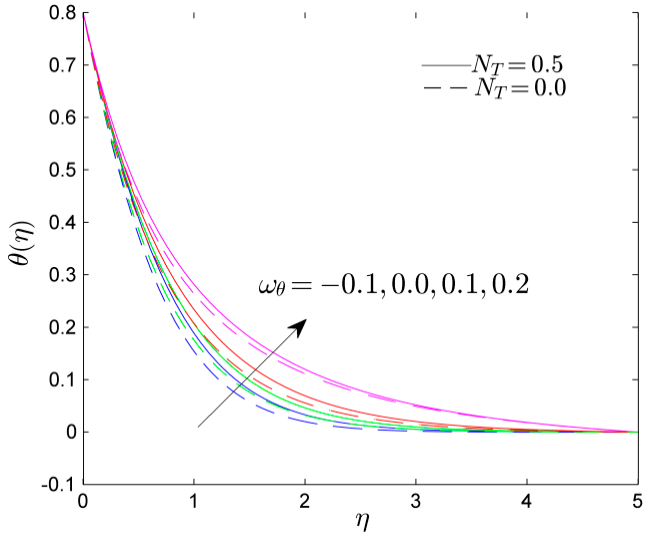

Figure 14. Effect of thermal relaxation time parameter (ω_θ) on $\theta(\eta)$.

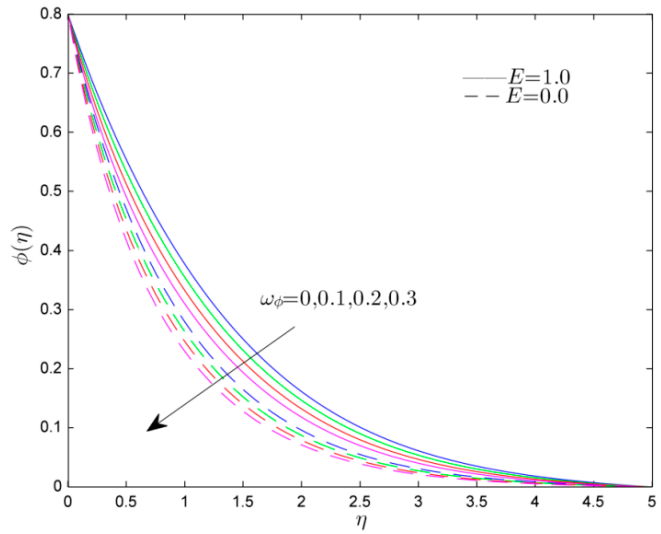

Figure 15. Effect of Mass relaxation parameter (ω_ϕ) on $\phi(\eta)$.

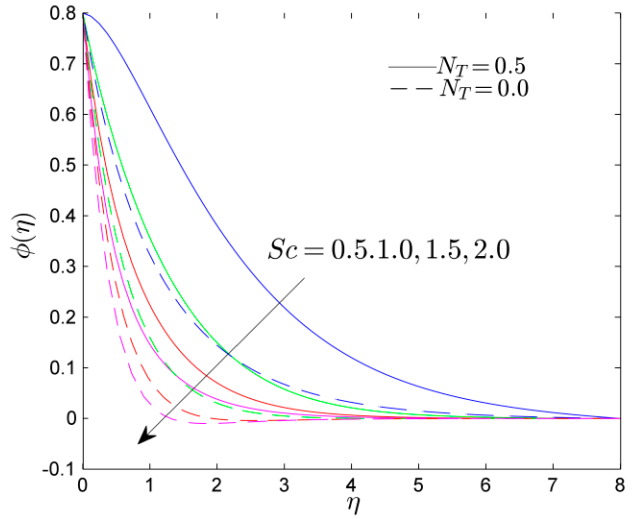

Figure 16. Effect of Schmidt number (Sc) on $\phi(\eta)$.

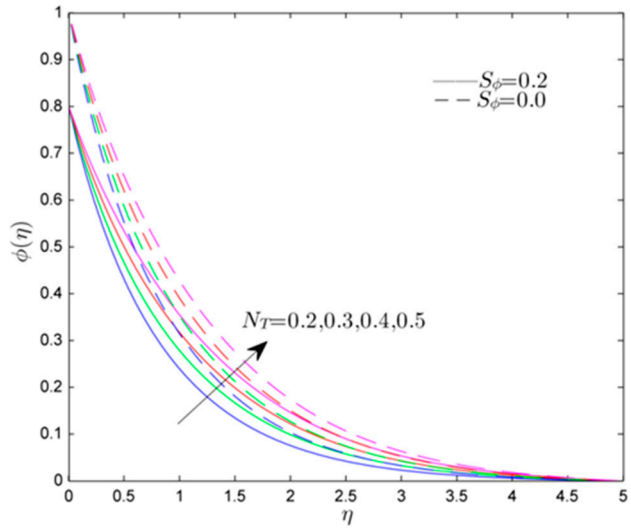

Figure 17. Effect of Thermophoresis parameter (N_T) on $\phi(\eta)$.

Figures 18–20 show the role of numerous parameters on skin friction coefficients and heat and mass transfer rates. We concluded from Figure 18a,b that the skin friction coefficient rises at *fw* and *Wi* while also increasing in *Ri* and *Wi*. Figure 19a,b display a lower Nusselt number due to a lower R and ω_θ as well as diminished N_T and S_θ. Figure 20a,b depict the mass diffusion rate for various estimates of *fw* and S_ϕ. The mass diffusion rate increased in this case as the values of *fw* and S_ϕ increased, and *Sc* and ω_ϕ also increased.

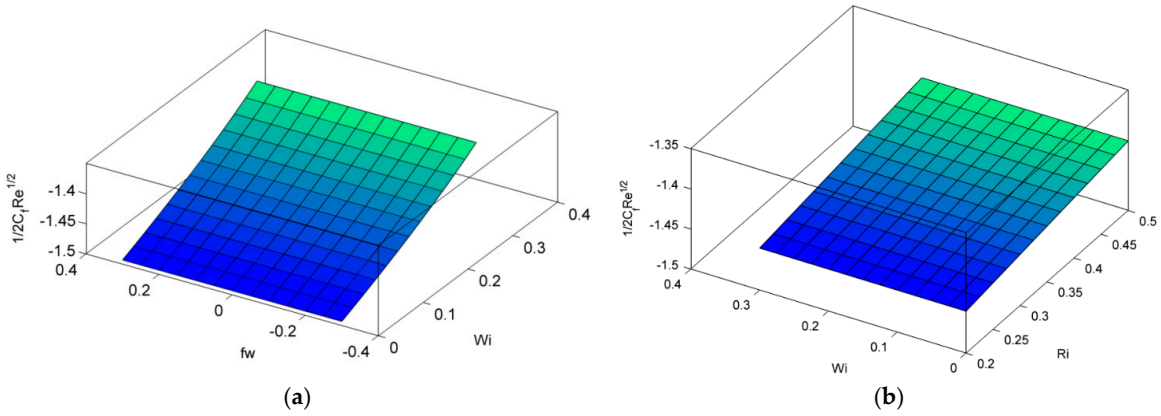

(**a**) (**b**)

Figure 18. Three-dimensional plots of skin friction for (**a**) fw and Wi, (**b**) Ri, and Wi.

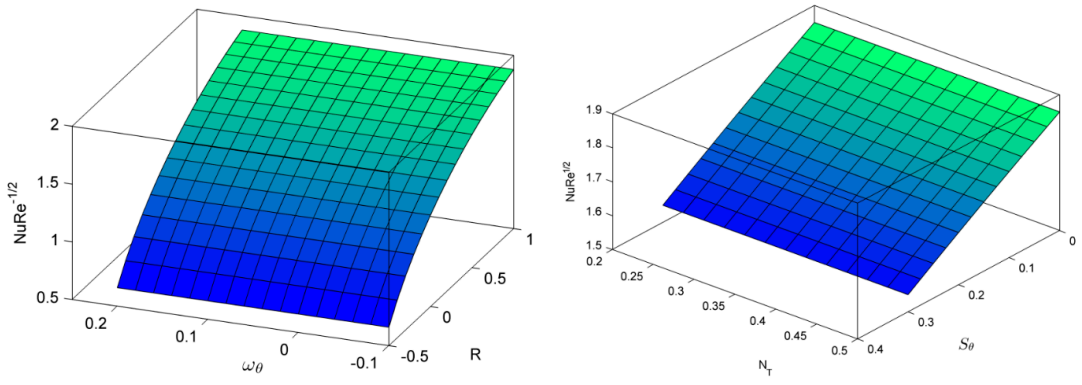

(**a**) (**b**)

Figure 19. 3D plot of Nusselt number for (**a**) R and ω_θ, (**b**) N_T and S_θ.

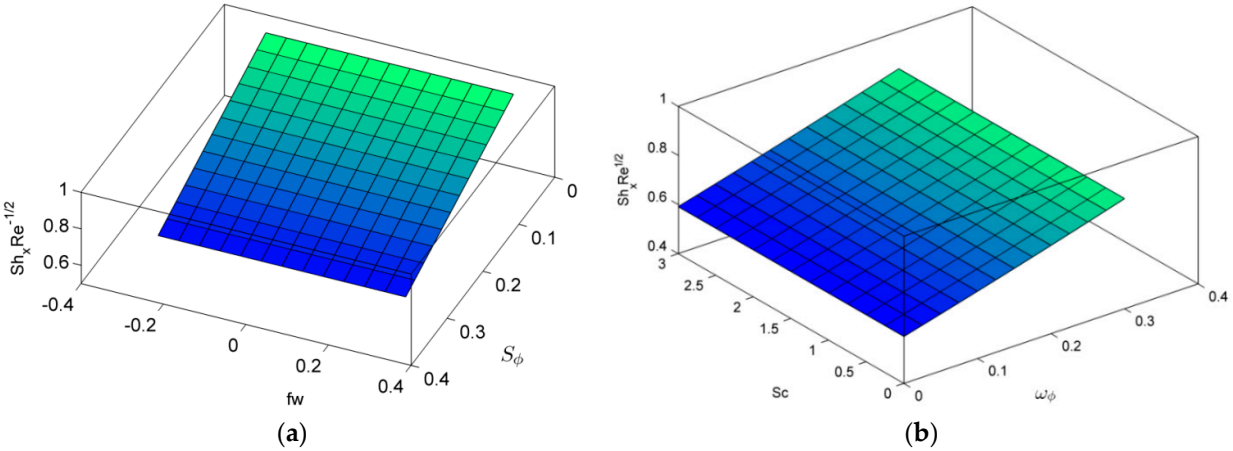

Figure 20. The 3D plot of Sherwood number for (**a**) fw and S_ϕ, (**b**) Sc and ω_ϕ.

5. Conclusions

The numerical and analytical results of the Darcy–Forchheimer Williamson nanofluid flow through a linear stretched surface were observed in this paper. In addition, the effects of thermal and solutal stratification, activation energy, and the Cattaneo–Christov dual flux were all considered. The following are the outcomes of this work.

i. The velocity profile was reduced by the Weissenberg number and Forchheimer number, while the mixed convective parameter shows the increasing tendency in velocity profile.
ii. The temperature distribution was raised with a high thermal relaxation time and radiation values.
iii. For higher estimations of Schmidt number and mass relaxation time, the concentration profile diminished.
iv. Increases in the thermal and mass stratification parameters reduce the temperature and concentration profile.
v. Heat and mass transfer rates were declined for large values of thermal radiation, thermal relaxation time, mass stratification, and suction parameter.

The findings discussed in this work should benefit scientists and engineers in various chemical and thermal engineering applications such as nuclear reactors, cooling systems, and hybrid power systems.

Author Contributions: Conceptualization, B.M.T. and S.K.; methodology, B.M.T. and M.K.A.K.; software, B.M.T.; validation, B.M.T., M.Y. and F.Ö.; formal analysis, S.K. and M.Y.; investigation, S.K. and M.K.A.K.; resources, M.Y. and F.Ö.; data curation, S.K.; writing—original draft, B.M.T.; writing—review and editing, B.M.T. and S.K.; visualization, M.Y. and F.Ö.; supervision, S.K. and M.K.A.K.; project administration, M.Y. and F.Ö.; funding acquisition, M.Y., M.K.A.K. and F.Ö. All authors have read and agreed to the published version of the manuscript.

Funding: This research received no external funding.

Acknowledgments: The authors are grateful to "Research and Development Wing, Live4Research, Tiruppur, Tamilnadu, India" for the valuable support throughout this project work. Fatma Özköse was supported by Research Fund of the Erciyes University. Project number: FDS-2021-11059.

Conflicts of Interest: The authors declare no conflict of interest.

Abbreviations

List of Symbols

a	Stretching rate	(s^{-1})
C_B	Drag coefficient	
C_p	Specific heat	$(Jkg^{-1}k^{-1})$
B_0	Magnetic field	$(kgs^{-2}A^{-1})$
C_w	Surface concentration	(kgm^{-3})
lg	Acceleration due to gravity	(ms^{-2})
C_∞	Ambient fluid concentration	(kgm^{-3})
lD_B	Mass diffusivity	(m^2s^{-1})
C	Fluid concentration	(kgm^{-3})
D_T	Thermophoretic diffusion coefficient	(m^2s^{-1})
$E = (E_A/kT_\infty)$	Activation energy	Dimensionless
$Fc=\left(C_B/\sqrt{k_f}\right)$	Forchheimer number	Dimensionless
$Gr = \left(\frac{(g\beta(1-C_\infty)(T_w-T_\infty)x^3)}{\vartheta^2}\right)$	Local Grashof number	Dimensionless
$H_A = \left(Q_1/\rho_f C_p a\right)$	Heat generation parameter	Dimensionless
k	Thermal conductivity	$\left(Wm^{-1}k^{-1}\right)$
k_f	Permeability of porous medium	Dimensionless
$fw = -\left(V_w/\sqrt{a\vartheta}\right)$	Suction/injection parameter	Dimensionless
k_p	Mean absorption coefficient	Dimensionless
k_r	Reaction rate	Dimensionless
$M = \left(\sigma B_0^2/\rho_f a\right)$	Magnetic parameter	Dimensionless
n	Fitted rate	Dimensionless
N_B=$(\tau D_B C_\infty/\vartheta)$	Brownian diffusion parameter	Dimensionless
$B_N = \left(\frac{(\rho_p-\rho_{f\infty})C_\infty}{\rho_{f\infty}\wedge_1(1-C_\infty)(T_w-T_0))}\right)$	Buoyancy ratio parameter	Dimensionless
$Pr = \left(k_f/(\rho c)_f\right)$	Prandtl number	Dimensionless
$Re_x = (U_w x/\vartheta)$	Local Reynolds number	Dimensionless
$\lambda = \left(\frac{Gr}{Re_x^2}\right) = \left(\frac{(g\wedge_1(1-C_\infty)(T_w-T_\infty))}{a^2x}\right)$	Richardson number	Dimensionless
$Sc = (\vartheta/D_B)$	Schmidt number	Dimensionless
T	Fluid temperature	(K)
$Wi = \left(\wedge x\sqrt{2a^3/\vartheta}\right)$	Weissenberg number	Dimensionless
T_∞	Ambient temperature	(K)
u and v	Velocity components	(ms^{-1})
U_w	Stretching surface velocity	(ms^{-1})
S_θ	Thermal stratification	Dimensionless
x and y	Direction coordinates	(m)
S_ϕ	Solutal stratification	Dimensionless
T_w	Wall temperature	(K)
$N_T = \left(\frac{\tau D_T(T_w-T_0)}{T_\infty\vartheta}\right)$	Thermophoresis parameter	Dimensionless
$R = \left(4\sigma^* T_\infty^3/k_p k_f\right)$	Thermal Radiation	Dimensionless
$\rho_f C_p$	Heat capacity	$(Jk^{-1}m^{-3})$

Greek Symbols

$\omega_\theta = (a\Gamma_T)$	Thermal relaxation time parameter	Dimensionless
$\delta = \left(\frac{(T_w-T_0)}{T_\infty}\right)$	Temperature difference parameter	Dimensionless
$\omega_\phi = (a\Gamma_C)$	Mass relaxation parameter	Dimensionless
ρ_f	Fluid density	(kgm^{-3})
α	Thermal diffusivity	(m^2s^{-1})
$\wedge$	Williamson parameter	Dimensionless
θ	Non dimensional temperature	Dimensionless
ϕ	Non dimensional concentration	Dimensionless
σ_0	Dimensionless reaction rate	Dimensionless

References

1. Choi, S. Enhancing thermal conductivity of fluids with nanoparticles. In Proceedings of the ASME International Mechanical Engineering Congress & Exposition, San Francisco, CA, USA, 12–17 November 1995; pp. 99–105.
2. Buongiorno, J. Convective transport in nanofluids. *J. Heat Transf.* **2006**, *128*, 240–250. [CrossRef]
3. Williamson, R.V. The Flow of Pseudoplastic Materials. *Ind. Eng. Chem.* **1929**, *21*, 1108–1111. [CrossRef]
4. Nadeem, S.; Hussain, S.T.; Lee, C. Flow of a Williamson fluid over a stretching sheet. *Braz. J. Chem. Eng.* **2013**, *30*, 619–625. [CrossRef]
5. Hayat, T.; Shafiq, A.; Alsaedi, A. Hydromagnetic boundary layer flow of Williamson fluid in the presence of thermal radiation and Ohmic dissipation. *Alex. Eng. J.* **2016**, *55*, 2229–2240. [CrossRef]
6. Karthikeyan, S.; Bhuvaneswari, M.; Sivasankaran, S.; Rajan, S. Cross diffusion, radiation and chemical reaction effects on MHD combined convective flow towards a stagnation-point upon vertical plate with heat generation. *IOP Conf. Ser. Mater. Sci. Eng.* **2018**, *390*, 012088. [CrossRef]
7. Zeeshan, A.; Shehzad, N.; Atif, M.; Ellahi, R. SS symmetry Electromagnetic Flow of SWCNT/MWCNT Suspensions in Two Immiscible Water- and Engine-Oil-Based Newtonian Fluids through Porous Media. *Symmetry* **2022**, *14*, 406. [CrossRef]
8. Ahmed, K.; Akbar, T.; Muhammad, T. Physical Aspects of Homogeneous–Heterogeneous Reactions on MHD Williamson Fluid Flow across a Nonlinear Stretching Curved Surface Together with Convective Boundary Conditions. *Math. Probl. Eng.* **2021**, *2021*, 7016961. [CrossRef]
9. Waqas, H.; Farooq, U.; Ali, S.; Hashim, K.; Marjan, M.A. Numerical analysis of dual variable of conductivity in bioconvection flow of Carreau–Yasuda nanofluid containing gyrotactic motile microorganisms over a porous medium. *J. Therm. Anal. Calorim.* **2021**, *145*, 2033–2044. [CrossRef]
10. Shehzad, N.; Zeeshan, A.; Shakeel, M.; Ellahi, R.; Sait, S.M. Effects of Magnetohydrodynamics Flow on Multilayer Coatings of Newtonian and Non-Newtonian Fluids through Porous Inclined Rotating Channel. *Coatings* **2022**, *12*, 430. [CrossRef]
11. Loganathan, K.; Mohana, K.; Mohanraj, M.; Sakthivel, P.; Rajan, S. Impact of third-grade nanofluid flow across a convective surface in the presence of inclined Lorentz force: An approach to entropy optimization. *J. Therm. Anal. Calorim.* **2020**, *144*, 1935–1947. [CrossRef]
12. Yusuf, T.A.; Mabood, F.; Prasannakumara, B.C.; Sarris, I.E. Magneto-bioconvection flow of Williamson nanofluid over an inclined plate with gyrotactic microorganisms and entropy generation. *Fluids* **2021**, *6*, 109. [CrossRef]
13. Qureshi, M.A. Numerical simulation of heat transfer flow subject to MHD of Williamson nanofluid with thermal radiation. *Symmetry* **2021**, *13*, 10. [CrossRef]
14. Salahuddin, T.; Malik, M.Y.; Hussain, A.; Bilal, S.; Awais, M. MHD flow of Cattaneo–Christov heat flux model for Williamson fluid over a stretching sheet with variable thickness: Using numerical approach. *J. Magn. Magn. Mater.* **2016**, *401*, 991–997. [CrossRef]
15. Qayyum, S.; Khan, M.I.; Hayat, T.; Alsaedi, A.; Tamoor, M. Entropy generation in dissipative flow of Williamson fluid between two rotating disks. *Int. J. Heat Mass Transf.* **2018**, *127*, 933–942. [CrossRef]
16. Hayat, T.; Qayyum, A.; Alsaedi, A. Three-dimensional mixed convection squeezing flow. *Appl. Math. Mech.* **2015**, *36*, 47–60. [CrossRef]
17. Ibrahim, W.; Negara, M. Viscous dissipation effect on mixed convective heat transfer of MHD flow of Williamson nanofluid over a stretching cylinder in the presence of variable thermal conductivity and chemical reaction. *Heat Transf.* **2021**, *50*, 2427–2453. [CrossRef]
18. Khan, W.A.; Khan, M.; Alshomrani, A.S.; Ahmad, L. Numerical investigation of generalized Fourier's and Fick's laws for Sisko fluid flow. *J. Mol. Liq.* **2016**, *224*, 1016–1021. [CrossRef]
19. Eswaramoorthi, S.; Loganathan, K.; Jain, R.; Gyeltshen, S. Darcy-Forchheimer 3D Flow of Glycerin-Based Carbon Nanotubes on a Riga Plate with Nonlinear Thermal Radiation and Cattaneo–Christov Heat Flux. *J. Nanomater.* **2022**, *2022*, 5286921. [CrossRef]
20. Conduzionedelcalore, C.C.S. Atti del Seminario Matematico e Fisico dell'Universita di Modena e Reggio Emilia. *Modena by Seminario matematico e fisico Università di Modena* **1948**, *3*, 83–101.
21. Christov, C.I. On frame indifferent formulation of the Maxwell–Cattaneo model of finite-speed heat conduction. *Mech. Res. Commun.* **2009**, *36*, 481–486. [CrossRef]
22. Eswaramoorthi, S.; Alessa, N.; Sangeethavaanee, M.; Namgyel, N. Numerical and Analytical Investigation for Darcy-Forchheimer Flow of a Williamson fluid over a Riga Plate with Double Stratification and Cattaneo–Christov Dual Flux. *Adv. Math. Phys.* **2021**, *2021*, 1867824. [CrossRef]
23. Hayat, T.; Khan, M.I.; Farooq, M.; Alsaedi, A.; Waqas, M.; Yasmeen, T. Impact of Cattaneo–Christov heat flux model inflow of variable thermal conductivity fluid over a variable thicked surface. *Int. J. Heat Mass Transf.* **2016**, *99*, 702–710. [CrossRef]
24. Shankar, B. Goud Heat generation/absorption influence on steady stretched permeable surface on MHD flow of a micropolar fluid through a porous medium in the presence of variable suction/injection. *Int. J. Thermofluids* **2020**, *7–8*, 100044. [CrossRef]
25. Ali, B.; Nie, Y.; Hussain, S.; Manan, A.; Sadiq, M.T. Unsteady magneto-hydrodynamic transport of rotating Maxwell nanofluid flow on a stretching sheet with Cattaneo–Christov double diffusion and activation energy. *Therm. Sci. Eng. Prog.* **2020**, *20*, 100720. [CrossRef]
26. Abu-Hamden, N.H.; Alsulami, R.A.; Rawa, M.J.H.; Alazwari, M.A.; Goodarzi, M.; Safaei, M.R. A Significant Solar Energy Note on Powell-Eyring Nanofluid with Thermal Jump Conditions: Implementing Cattaneo–Christov Heat Flux Model. *Mathematics* **2021**, *9*, 669. [CrossRef]

27. Rashid, S.; Khan, M.I.; Hayat, T.; Ayub, M.; Alsaedi, A. Darcy–Forchheimer flow of Maxwell fluid with activation energy and thermal radiation over an exponential surface. *Appl. Nanosci.* **2020**, *10*, 2965–2975. [CrossRef]
28. Shafiq, A.; Rasool, G.; Khalique, C.M. Significance of thermal slip and convective boundary conditions in three dimensional rotating darcy-forchheimer nanofluid flow. *Symmetry* **2020**, *12*, 741. [CrossRef]
29. Rasool, G.; Zhang, T.; Chamkha, A.J.; Shafiq, A.; Tlili, I.; Shahzadi, G. Entropy generation and consequences of binary chemical reaction on mhd darcy-forchheimer Williamson nanofluid flow over non-linearly stretching surface. *Entropy* **2020**, *22*, 18. [CrossRef]
30. Hayat, T.; Aziz, A.; Muhammad, T.; Alsaedi, A. Darcy–Forchheimer Three-Dimensional Flow of Williamson Nanofluid over a Convectively Heated Nonlinear Stretching Surface. *Commun. Theor. Phys.* **2017**, *68*, 387–394. [CrossRef]
31. Bestman, A.R. Natural convection boundary layer with suction mass transfer in a porous medium. *Int. J. Energy Res.* **1990**, *14*, 389–396. [CrossRef]
32. Dawar, A.; Shah, Z.; Islam, S. Mathematical modeling and study of MHD flow of Williamson nanofluid over a nonlinear stretching plate with activation energy. *Heat Transf.* **2021**, *50*, 2558–2570. [CrossRef]
33. Alsaadi, F.E.; Hayat, T.; Khan, M.I.; Alsaadi, F.E. Heat transport and entropy optimization inflow of magneto-Williamson nanomaterial with Arrhenius activation energy. *Comput. Methods Programs Biomed.* **2020**, *183*, 105051. [CrossRef]
34. Muhammad, R.; Khan, M.I.; Jameel, M.; Khan, N.B. Fully developed Darcy-Forchheimer mixed convective flow over a curved surface with activation energy and entropy generation. *Comput. Methods Programs Biomed.* **2020**, *188*, 105298. [CrossRef] [PubMed]
35. Danook, S.H.; Jasim, Q.K.; Hussein, A.M. Nanofluid Convective Heat Transfer Enhancement Elliptical Tube inside Circular Tube under Turbulent Flow. *Math. Comput. Appl.* **2018**, *23*, 78. [CrossRef]
36. Jamshed, W.; Goodarzi, M.; Prakash, M.; Nisar, K.S.; Zakarya, M.; Abdel-Aty, A.H. Evaluating the unsteady Casson nanofluid over a stretching sheet with solar thermal radiation: An optimal case study. *Case Stud. Therm. Eng.* **2021**, *26*, 101160. [CrossRef]
37. Alghamdi, M.; Wakif, A.; Thumma, T.; Khan, U. Case Studies in Thermal Engineering Significance of variability in magnetic field strength and heat source on the radiative-convective motion of sodium alginate-based nanofluid within a Darcy-Brinkman porous structure bounded vertically by an irregular slender surface. *Case Stud. Therm. Eng.* **2021**, *28*, 101428. [CrossRef]
38. Loganathan, K.; Rajan, S. An entropy approach of Williamson nanofluid flow with Joule heating and zero nanoparticle mass flux. *J. Therm. Anal. Calorim.* **2020**, *141*, 2599–2612. [CrossRef]
39. Ibrahim, W.; Negara, M. The Investigation of MHD Williamson Nanofluid over Stretching Cylinder with the Effect of Activation Energy. *Adv. Math. Phys.* **2020**, *2020*, 9523630. [CrossRef]
40. Sajid, T.; Tanveer, S.; Sabir, Z.; Guirao, J.L.G. Impact of Activation Energy and Temperature-Dependent Heat Source/Sink on Maxwell-Sutterby Fluid. *Math. Probl. Eng.* **2020**, *2020*, 5251804. [CrossRef]
41. Zaib, A.; Abelman, S.; Chamkha, A.J.; Rashidi, M.M. Entropy Generation of Williamson Nanofluid near a Stagnation Point over a Moving Plate with Binary Chemical Reaction and Activation Energy. *Heat Transf. Res.* **2018**, *49*, 1131–1149. [CrossRef]
42. Hayat, T.; Aziz, A.; Muhammad, T.; Alsaedi, A. Effects of binary chemical reaction and Arrhenius activation energy in Darcy–Forchheimer three-dimensional flow of nanofluid subject to rotating frame. *J. Therm. Anal. Calorim.* **2019**, *136*, 1769–1779. [CrossRef]
43. Ibrahim, W.; Negara, M. Viscous dissipation effect on Williamson nanofluid over stretching/ shrinking wedge with thermal radiation and chemical reaction. *J. Phys. Commun.* **2020**, *4*, 045015. [CrossRef]
44. Ramzan, M.; Gul, H.; Kadry, S.; Chu, Y.M. Role of bioconvection in a three dimensional tangent hyperbolic partially ionized magnetized nanofluid flow with Cattaneo–Christov heat flux and activation energy. *Int. Commun. Heat Mass Transf.* **2021**, *120*, 104994. [CrossRef]
45. Kumar, R.; Sood, S.; Shehzad, S.A.; Sheikholeslami, M. Radiative heat transfer study for flow of non-Newtonian nanofluid past a Riga plate with variable thickness. *J. Mol. Liq.* **2017**, *248*, 143–152. [CrossRef]
46. Khan, W.A.; Khan, M.; Alshomrani, A.S. Impact of chemical processes on 3D Burgers fluid utilizing Cattaneo–Christov double-diffusion: Applications of non-Fourier's heat and non-Fick's mass flux models. *J. Mol. Liq.* **2016**, *223*, 1039–1047. [CrossRef]
47. Hayat, T.; Muhammad, K.; Farooq, M.; Alsaedi, A. Squeezed flow subject to Cattaneo–Christov heat flux and rotating frame. *J. Mol. Liq.* **2016**, *220*, 216–222. [CrossRef]
48. Loganathan, K.; Alessa, N.; Kayikci, S. Heat Transfer Analysis of 3-D Viscoelastic Nano-fluid Flow Over a Convectively Heated Porous Riga Plate with Cattaneo–Christov Double Flux. *Front. Phys.* **2021**, *9*, 1–12. [CrossRef]
49. Karthik, T.S.; Loganathan, K.; Shankar, A.N.; Carmichael, M.J.; Mohan, A.; Kaabar, M.K.A.; Kayikci, S. Zero and Nonzero Mass Flux Effects of Bioconvective Viscoelastic Nanofluid over a 3D Riga Surface with the Swimming of Gyrotactic Microorganisms. *Adv. Math. Phys.* **2021**, *2021*, 9914134. [CrossRef]
50. Ahmad, A.G.; Kaabar, M.K.A.; Rashid, S.; Abid, M. A Novel Numerical Treatment of Nonlinear and Nonequilibrium Model of Gradient Elution Chromatography considering Core-Shell Particles in the Column. *Math. Probl. Eng.* **2022**, *2022*, 1619702. [CrossRef]
51. Yavuz, M.; Sene, N.; Yıldız, M. Analysis of the Influences of Parameters in the Fractional Second-Grade Fluid Dynamics. *Mathematics* **2022**, *10*, 1125. [CrossRef]
52. Islam, T.; Yavuz, M.; Parveen, N.; Fayz-Al-Asad, M. Impact of Non-Uniform Periodic Magnetic Field on Unsteady Natural Convection Flow of Nanofluids in Square Enclosure. *Fractal Fract.* **2022**, *6*, 101. [CrossRef]

53. Fayz-Al-Asad, M.; Yavuz, M.; Alam, M.; Sarker, M.; Alam, M.; Bazighifan, O. Influence of fin length on magneto-combined convection heat transfer performance in a lid-driven wavy cavity. *Fractal Fract.* **2021**, *5*, 107. [CrossRef]
54. Sene, N. Second-grade fluid with Newtonian heating under Caputo fractional derivative: Analytical investigations via Laplace transforms. *Math. Model. Numer. Simul. Appl.* **2022**, *2*, 13–25. [CrossRef]
55. Khan, A.; Khan, A.; Sinan, M. Ion temperature gradient modes driven soliton and shock by reduction perturbation method for electron-ion magneto-plasma. *Math. Model. Numer. Simul. Appl.* **2022**, *2*, 1–12. [CrossRef]
56. Sreelakshmi, K.; Sarojamma, G.; Makinde, O.D. Dual stratification on the Darcy–Forchheimer flow of a maxwell nanofluid over a stretching surface. In *Defect and Diffusion Forum*; Trans Tech Publications Ltd.: Freienbach, Switzerland, 2018; Volume 387, pp. 207–217. [CrossRef]
57. Hayat, T.; Shah, F.; Hussain, Z.; Alsaedi, A. Outcomes of double stratification in Darcy–Forchheimer MHD flow of viscoelastic nanofluid. *J. Brazilian Soc. Mech. Sci. Eng.* **2018**, *40*, 145. [CrossRef]
58. Eswaramoorthi, S.; Alessa, N.; Sangeethavaanee, M.; Kayikci, S.; Namgyel, N. Mixed Convection and Thermally Radiative Flow of MHD Williamson Nanofluid with Arrhenius Activation Energy and Cattaneo–Christov Heat-Mass Flux. *J. Math.* **2021**, *2021*, 2490524. [CrossRef]
59. Ahmed, K.; Khan, W.A.; Akbar, T.; Rasool, G.; Alharbi, S.O.; Khan, I. Numerical Investigation of Mixed Convective Williamson Fluid Flow Over an Exponentially Stretching Permeable Curved Surface. *Fluids* **2021**, *6*, 260. [CrossRef]
60. Ramzan, M.; Gul, H.; Darcy-Forchheimer, M.Z. 3D Williamson nanofluid flow with generalized Fourier and Fick's laws in a stratified medium. *Bull. Polish Acad. Sci. Technol. Sci.* **2020**, *68*, 327–335. [CrossRef]
61. Haider, F.; Hayat, T.; Alsaedi, A. Flow of hybrid nanofluid through Darcy-Forchheimer porous space with variable characteristics. *Alex. Eng. J.* **2021**, *60*, 3047–3056. [CrossRef]
62. Irfan, M.; Khan, M. Simultaneous impact of nonlinear radiative heat flux and Arrhenius activation energy inflow of chemically reacting Carreau nanofluid. *Appl. Nanosci.* **2020**, *10*, 2977–2988. [CrossRef]
63. Hayat, T.; Naz, S.; Waqas, M.; Alsaedi, A. Effectiveness of Darcy-Forchheimer and nonlinear mixed convection aspects in stratified Maxwell nanomaterial flow induced by convectively heated surface. *Appl. Math. Mech.* **2018**, *39*, 1373–1384. [CrossRef]
64. Kumar, K.A.; Reddy, J.V.R.; Sugunamma, V.; Sandeep, N. MHD Carreau fluid flow past a melting surface with Cattaneo–Christov heat flux. In *Applied Mathematics and Scientific Computing*; Trends in Mathematics; Birkhäuser: Cham, Switzerland, 2019; pp. 325–336. [CrossRef]
65. Hayat, T.; Muhammad, T.; Shehzad, S.A.; Alsaedi, A.; Al-Solamy, F. Radiative Three-Dimensional Flow with Chemical Reaction. *Int. J. Chem. React. Eng.* **2016**, *14*, 79–91. [CrossRef]
66. Sahoo, A.; Nandkeolyar, R. Entropy generation in convective radiative flow of a Casson nanofluid in non-Darcy porous medium with Hall current and activation energy: The multiple regression model. *Appl. Math. Comput.* **2021**, *402*, 125923. [CrossRef]
67. Chu, Y.M.; Nazeer, M.; Khan, M.I.; Ali, W.; Zafar, Z.; Kadry, S.; Abdelmalek, Z. Entropy analysis in the Rabinowitsch fluid model through inclined Wavy Channel: Constant and variable properties. *Int. Commun. Heat Mass Transf.* **2020**, *119*, 104980. [CrossRef]
68. Hayat, T.; Javed, M.; Imtiaz, M.; Alsaedi, A. Double stratification in the MHD flow of a nanofluid due to a rotating disk with variable thickness. *Eur. Phys. J. Plus* **2017**, *132*, 146. [CrossRef]
69. Mustafa, M.; Khan, J.A.; Hayat, T.; Alsaedi, A. Buoyancy Effects on the MHD nanofluid flow past a vertical surface with chemical reaction and activation energy. *Int. J. Heat Mass Transf.* **2017**, *108*, 1340–1346. [CrossRef]
70. Loganathan, K.; Alessa, N.; Namgyel, N.; Karthik, T.S. MHD Flow of Thermally Radiative Maxwell Fluid Past a Heated Stretching Sheet with Cattaneo—Christov Dual Diffusion. *J. Math.* **2021**, *2021*, 5562667. [CrossRef]